ORIGINAL ARTICLE

Spacecraft Materials' Reflectivity and Surface Morphology: Aging Caused by Proton Irradiation

Denise Keil[1] · **Maciej Sznajder[2,3]** · **Thomas Renger[3]** · **Nils Bartels[1]** ·
Patric Seefeldt[3] · **Wolfgang Riede[1]** · **Tom Spröwitz[3]** · **Thomas Dekorsy[1]**

© The Author(s) 2023

Abstract

The radiation environment in Low Earth Orbit (LEO) is dominated by protons captured by Earth's magnetic field in the Inner Van-Allen belt. Defunct satellites and other space debris objects can be resident in this environment for several decades and even centuries. So far, there is little knowledge about the impact of long-duration proton exposure to the surface morphology and reflectivity in LEO environment. We report on a laboratory test campaign exposing typical spacecraft materials with protons of 100 keV and 2.5 keV kinetic energy and a fluence corresponding to an in-orbit duration of 100 years and 120 years, respectively, in an 800 km sunsynchronous orbit. Although we find microscopic changes in surface morphology, reflectivity changes of all tested materials were smaller than 15%. This result brings positive news for on-going efforts to use optical methods, e.g. lightcurve measurements or active polarimetry, for characterizing space objects, since it suggests that data can - to a good approximation - be analyzed without accounting for proton induced aging effects that might affect the materials' optical properties over time.

Keywords Space aging · Space debris · Object characterization · Complex irradiation facility · Protons · Orbital environment models

Maciej Sznajder, Thomas Renger, Nils Bartels and Patric Seefeldt have contributed equally to this work.

✉ Denise Keil
   denise.keil@dlr.de

✉ Maciej Sznajder
   Maciej.Sznajder@p3run.com

1   Institute of Technical Physics, German Aerospace Center, Pfaffenwaldring 38-40, Stuttgart 70569, Germany

2   PW Sznajder, P3RUN - Radiation Hardness Assurance & Data Science Expertise, Dolina Zielona 19A, Zielona Góra 65-154, Poland

3   Institute of Space Systems, German Aerospace Center, Robert-Hooke-Strasse 7, Bremen 28359, Germany

🙋 Springer

1 Introduction

Frequently, avoidance maneuvers or damages on the International Space Station (ISS) or famous satellite missions are on the news due to space debris [1, 10, 11, 31, 32]. For example, the ISS robotic arm, Canadarm, was hit by space debris particles during spring 2021 [29]. The impressive hole in the blankets luckily does not influence the functionality of the service. More cost intensive was the damage at the cooling system of a Soyuz capsule in December 2022. An interaction with space debris is not excluded from the list of potential causes [33]. Even if the cause of damage is not finally clarified, the option of a space debris interaction demonstrates the potential dangers very well. As the capsule was not considered to be safe, another capsule was launched to take the crew back to Earth [16]. As one can see, accurate knowledge about the space debris environment in existence, motion, origin, and material composition are highly relevant for on-going space missions across all orbits.

The orbital environment is harsh, consisting of extreme thermal conditions, as well as corpuscular and electromagnetic radiation [19]. The environment very close to Earth, up to 700 km, is dominated by atomic oxygen (ATOX) which results from photodissociation effects of O_2 molecules on ultra-violet (UV) light [12, 23]. Thanks to experiments on the ISS, aging effects mainly due to ATOX are very well studied [2, 3]. In higher orbits, the Van-Allen-Belts take over with protons in the inner and electrons in the outer one [19]. Positioned between 0.2 to 2 Earth radii (spoken in L-Shells: L = 1 to L = 3) [8], the Inner Van-Allen-Belt intersects with the higher LEO orbits. As the dominant species in these orbits are protons, ranging between several keV to approximately 400 MeV, spacecrafts at 780 to 880 km sun-synchronous orbit are under exposure. Aside from the upcoming mega-constellations in lower orbits, this is the highest populated orbit among the higher ones [7]. Across all orbits debris that originates from the space environment occurs and potentially interacts with material surfaces. Such natural objects are for example micro-meteoroids and dust. Their interaction with artificial space objects can lead to abrasion and damage [15].

The Materials International Space Station Experiment (MISSE) series has tested over 4000 material samples and specimens - from lubricants and paints to fabrics, container seals and solar cell technologies - to test their durability in the space environment [21, 34]. In a sample return mission, the materials were brought back to Earth after 4 years exposure time. It was observed that many materials got destroyed, coatings changed or vanished [2, 3]. During a similar study on the Russian space station MIR by Skurat [28] aging effects on polymer films were studied. A conclusion of the study was that polytetrafluoroethylene based films suffer especially from ultra-violet wavelength while polyimide based films are predominantly damaged by ATOX. It was observed that materials become opaque and brittle [28]. Also, Engelhart et. al. [5, 6] show relevant impact of electron induced aging effects for geosynchronous (GEO) satellites. Relevant Materials were bombarded with electrons at 90 keV for an equivalent of between 1.6 and 5.5 GEO years depending on the material type. This, of course,

rises expectations of affecting optical data acquisition on space debris for lower LEO orbits.

Lightcurve data has recently generated growing interest. There is ongoing research to use optical methods (lightcurves modeling [20] and spectra-polarimetry [30]) to gain information on the material composition of space objects, e.g. for laser-based orbit modification via photon momentum transfer or material ablation [24–26]. For optical data modelling it is typically assumed that ground-based optical measurements of space materials before launch will not change when these materials are in orbit. Of course, this assumption needs to be carefully tested and thus, serves as a motivation for the present research.

In a previous study [14] we investigated proton-induced aging of space materials with proton irradiation at 100 keV with a fluence as expected to be accumulated during 100 years in an 800 km sun-synchronous orbit. The work presented here goes beyond that previous research by using an improved experimental setup. In this setup, only half the optical surface of each tested material is exposed to the radiation, whereas the other half is shielded with an aluminum cover. This allows for a direct comparison of exposed and unexposed areas on each sample, e.g. via microscopy and reflectivity measurements with a Fourier-Transform spectrometer. Furthermore, we expand our measurements to include an even lower proton energy of 2.5 keV. In that case, the energy will be dissipated within the first 100 nm on common spacecraft materials (at 100 keV protons will penetrate up to 1 μm) and is thus more likely to affect the surface properties. Since the previously used AP8 NASA standard model [12] for simulating the space environment is only valid for energies above 100 keV, we used the Onera GREEN (Global Radiation Earth ENvironment) model [27] to calculate the proton flux for proton kinetic energies down to 1 keV.

A microscopic inspection after proton exposure at 100 keV revealed that some tested spacecraft materials (the organic materials AcktarBlack and carbon fiber reinforced plastic) showed specific changes in the surface morphology. However, samples exposed to 2.5 keV proton irradiation showed no changes to the surface morphology, but small changes in reflectivity. These changes were 15% and less for all tested materials over the range of 0.5 to 2.3 μm. These are smaller than typical intensity variations in optical measurements, e.g. due to changes induced by turbulence [4, 13]. We thus conclude that the modeling of optical data (e.g. lightcurves) is - at least to a good approximation and for the set of tested materials and the simulated orbit - feasible without considering effects of proton-induced space aging.

2 Experiment

For the present study on proton-based space aging we used the Complex Irradiation Facility (CIF) at the DLR site in Bremen, Germany [22]. Several materials with relevance for space applications and with certain optical properties were chosen to be aged according the AP8 and GREEN model, respectively, and for a distinctive orbit and residential time conditions. Details will be discussed in the following subsections.

2.1 Complex Irradiation Facility CIF

The CIF [22] (see Fig. 1) is an Ultra High Vacuum facility equipped with two linear accelerators and three light sources to simulate the corpuscular (electrons and protons) and electromagnetic radiation of the Sun. The light sources are an Argon-VUV source, a Deuterium lamp, and a solar simulator equipped with a Xenon lamp.

The facility produces mono-energetic protons and electrons in a range from 2 keV to 100 keV. There is a common beam line from both accelerator sections which ends in the irradiation chamber where samples under study are located. Accelerators work in two modes, i.e. low energetic and high energetic. In the first one, electrons and protons can be produced within an energy range from 2 keV to 10 keV with a current up to 5 µA. In the high energetic mode, with an energy range from 10 keV to 100 keV, particle current can reach its maximum value of 100 µA.

The standard sample holder consists of two frames. The test sample will be clamped between the two parts. In this configuration an area of 36 cm^2 for irradiation is provided. A beam sweep mechanism is used in case of irradiation tests where the whole effective area is being exposed to protons or electrons. It consists of two pairs of plates located in the beam line. The beam sweeps over the test samples when a voltage with modulated amplitude is applied to the plates.

Electrons are produced by heating a LaB$_6$ cathode with well specified current parameters. The electrons are then accelerated to the required energy. Protons are generated by ionization of H$_2$ gas within a glass bulb by a radio frequency principle. The protons are then transported by a voltage to the acceleration section and further to the beamline. The acceleration section ends with bending magnets which bend
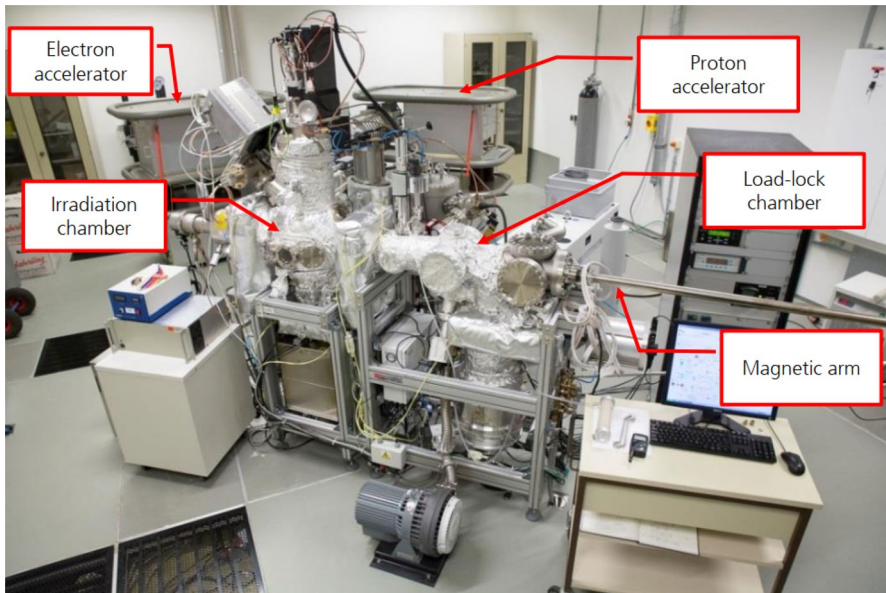

Fig. 1 Complex Irradiation Facility at DLR Bremen

the electron and proton beams into direction of the irradiation chamber where test specimens are located.

2.2 Radiation Conditions

Two experiments at different energy levels according to two different models have been conducted. Following up our previous experiment on proton aging [14], we chose to first simulate 100 keV according to the AP8 model [12] with an updated experimental set-up. 100 keV is the lowest possible energy which is covered by this model. Since more surface damage is expected to occur for even lower energies, we chose the Onera's GREEN model [27] which covers the energy spectrum down to 1 keV. Due to technical limitations of the CIF, the stability of the beam current at 1keV was not sufficient to provide the estimated fluences. In pre-tests, we iterated the settings, which finally lead to 2.5 keV as a minimum possible energy. For both models, flux and fluence spectra are plotted in Fig. 2. During the experiments, we simulated a space environment of the sun-synchronous orbit (SSO) for 800 km altitude. The equivalent orbital residence time was 100 years for 100 keV and 120 years for 2.5 keV, respectively.

2.3 Samples

During the experiment we were aiming to artificially age typical spacecraft materials (see Table 1) under common orbital conditions. Additionally, an X-Ray film
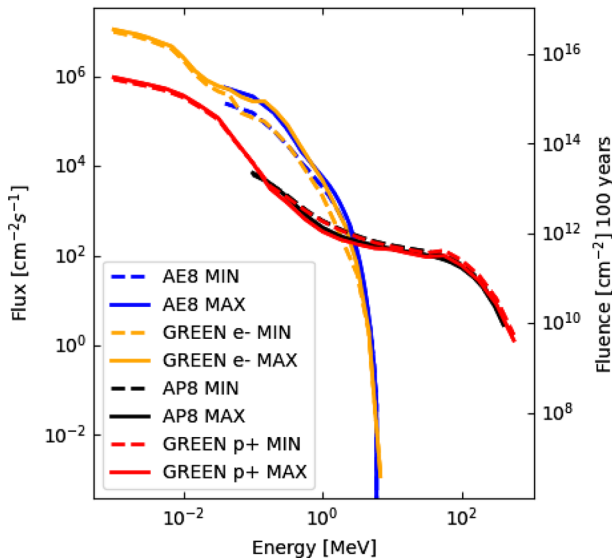

Fig. 2 Fluxes and fluences resulting from GREEN [27] (protons and electrons) and AP8/AE8 model [12], respectively, generated with SPENVIS [9]

Table 1 Choice of Sample Materials

Material	Thickness	Specification	Application
Carbon Fiber Reinforced Plastic (CFRP)	1 mm	Fiber Fabric with Epoxy resin, canvas woven	Black Polymer for satellite structures
AcktarBlack	125 μm aluminum coated with 3–7 μm carbon	Type: Spectral BlackTM, 99.5 - 99.7% absorptivity for wavelength range 0.3 - 14 μm	Substitute for carbon coated polymer and metal foils in optical applications and heat and charge radiators
Coated Polyimide	ca. 10 nm ITO - 25 μm Kapton - 100 nm aluminum	Type: Sheldahl No 146631, Stack: Indium Tin Oxide (ITO) - Kapton - Aluminum	Applied as component of passive thermal control system, so-called multi-layer insulation
Aluminum	2 mm	Standard metal material surface polished	Metal material for structural components in all types of spacecrafts
Titanium	0.8 mm	Metal material, surface polished	Metal material for structural components with special requirements regarding mechanical strength and restricted in weight and volume, e.g. tanks and brackets
Polytetrafluorethylene (PTFE, Teflon)	1 mm	Commercially available material, thickness	Polymer material with multiple applications, e.g. as coating, insulator or propellant

Table 2 Penetration depth d$_p$ per material and energy

Material	d$_p$(100 keV)	d$_p$(2.5 keV)
Carbon Fiber Reinforced Plastic (CFRP)	0.8 μm	47.0 nm
AcktarBlack	0.68 μm	40.1 nm
Coated Polyimide	1.04 μm	58.8 nm
Aluminum	0.83 μm	41.3 nm
Titanium	0.64 μm	32.7 nm
Polytetrafluorethylene (PTFE, Teflon)	1.17 μm	67.7 nm

Table 3 Measurement errors during the 100 keV irradiation procedure

Error Source	100 keV experiment	
	Nominal value	Error range
Swiped Sample Area	53.8 cm^2	$\pm$ 4.6 cm^2
Proton Current	100.4 nA	$\pm$ 2 nA
Exposure Time	2073 s	$\pm$ 1 s
Fluence	2.41×10^{13} p$^+$ cm^{-2}	$\pm 2.1 \times 10^{12}$ p$^+$ cm^{-2}
Equivalent Orbital Time	100 years	$\pm$9 years

sample was prepared as a reference. For each experiment we prepared a separate sample set. All samples of identical material originate from the same sheet and were following the same production process.

The expected surface damages during the experiment are related to the penetration depth. A small penetration depth means that more energy and charge is deposited close to the surface. Thus, more surface damage is expected. This is the reason for using the SRIM software [35] for penetration depths simulations and validated, as far as available, with PSTAR from National Institute of Standards and Technology (NIST) [18]. For the 100 keV experiment, the penetration depth ranges between 0.8 µm and 1.2 µm, while it lies between 32 nm and 68 nm for 2.5 keV proton irradiation. These results are summarized in Table 2.

2.4 Error Calculation

For the estimation of the uncertainty of our experiments, we conducted an error calculation, taking measurement inaccuracies and power fluctuations into account. The respective errors are listed in Tables 3 and 4.

2.5 Improvements in Comparison with Previous Experiments

During our first experiment in 2019 [14], the whole sample surface was exposed to the proton irradiation. After the experiment the aged sample surfaces were compared to a reference set of samples. To improve our interpretation of the aging results, we decided to create a solid anodized aluminum cover frame that

Table 4 Measurement errors during the 2.5 keV irradiation procedure

Error source	2.5 keV experiment	
	Nominal value	Error range
Swiped sample area	46.1 cm^2	±5.2 cm^2
Proton current	4.9 μA	±0.2 μA
Exposure time	5536 s	±1 s
Fluence	3.64×10^{15} p$^+$ cm^{-2}	$\pm 4.3 \times 10^{14}$ p$^+$ cm^{-2}
Equivalent orbital time	120 years	±14 years

prevents the right half of each sample from proton interaction. Figure 3 shows the updated sample holder. This improvement of the set-up provides us with a reference surface right next to the aged surface. This minimizes differences between reference and sample due to the production process as well as allows to compare surfaces that have experienced the exact same life circle. To avoid damages due to the cover frame, we installed it with a proper gap between the samples and the cover frame. All sample materials are on an aluminum base plate to ensure same surface level across the sample holder independently of the sample thickness.

3 Results

The aged samples have been investigated regarding their degradation. Here, we separated the effects on the surface structure and on the optical properties. After a proper examination of the samples of each energy level, the results for both were compared. The findings are discussed in the following.
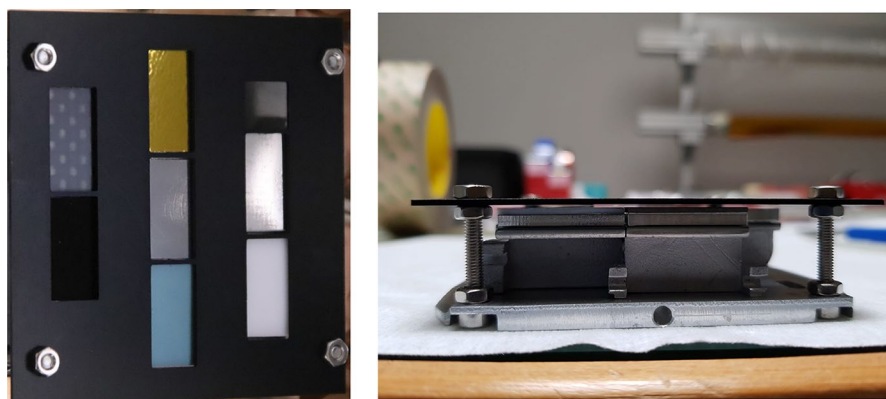
Fig. 3 Updated sample holder. Left: front perspective and Right: Side perspective

3.1 Aging Effects by Visual Inspection

After proton irradiation and relaxation time in the vacuum chamber, the samples were investigated by eye and changes were photo-documented. For the 100 keV test, no visible damages were accounted. The 2.5 keV test on the other hand showed significant changes on the surfaces of CFRP, coated polyimide, and X-Ray film samples. The changes appear as a slight change in color on the irradiated half of the samples. At the position, where the shielded sample halves and the exposed connect, a sudden change in contrast appears, which will further be referred to as "edge". Under UV illumination, a similar surface altering became visible for AcktarBlack. This is displayed in Fig. 4.

3.2 Mechanical Surface Degradation

Right after taking out the samples of the vacuum chamber, we investigated them with a Keyence Incident Light Microscope (see Appendix A.2.1). Before the irradiation process a stitch image of each surface was taken and compared to a stitch image after irradiation with same light conditions. Also, surface imperfections where captured and investigated prior to and after the irradiation.

For the 100 keV experiment, damage growth was found at two positions of the AcktarBlack surface, see Fig. 5. The microscopic view on the coated surface reveals an inhomogeneous structure of horizontal lighter and darker lines. These are in direction of the coating application on the aluminum base material and therefore an artifact of the production process. On the first position, the AcktarBlack coating is eroded and scratched significantly. The visible white lines are the aluminum base material. The shape and position of the imperfection fits the shape of the tweezers which were used to place the material on the sample holder, see Fig. 6. The second imperfection shows dark areas on the AcktarBlack surface. A closer look into the microscope reveals that the dark areas consist of fine black lining with random direction, see Fig. 7. It is expected that the AcktarBlack Coating got micro-cracks during the sample preparation process, since the imperfections are near the sample
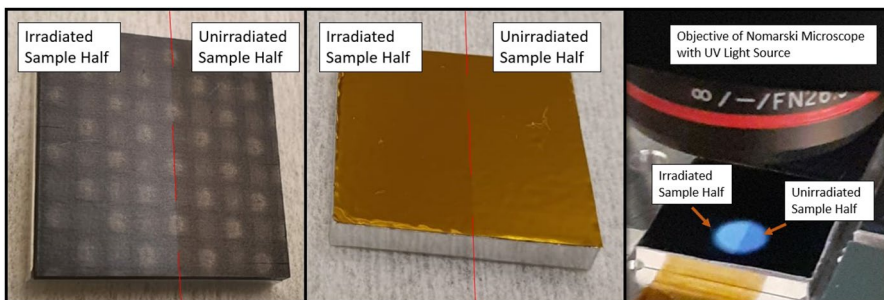

Fig. 4 Visible damages at samples after 2.5 keV proton irradiation equivalent 120 years. CFRP (left) and coated polyimide (middle) under laboratory lighting conditions, AcktarBlack (right) under UV illumination

Fig. 5 Stitch Image of AcktarBlack after irradiation with marked investigation areas with imperfections
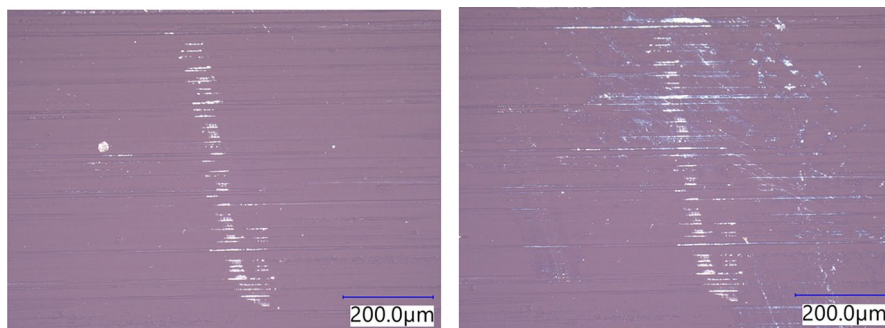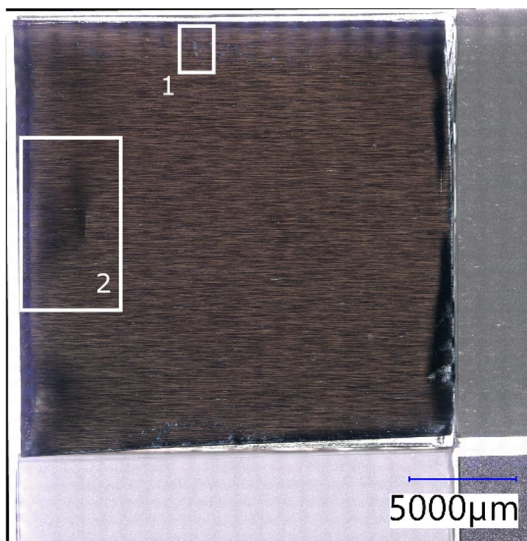

Fig. 6 Imperfection 1 in AcktarBlack before(left) and after (right) 100 keV proton irradiation
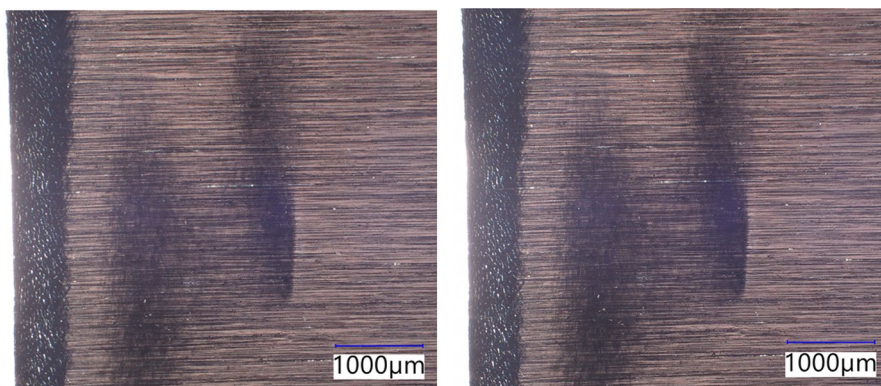

Fig. 7 Imperfection 2 in AcktarBlack before(left) and after (right) 100 keV proton irradiation

edge. As the sample is fixed to the sample holder, no further bending loads are to be expected. Therefore, an increasing number of cracks in the coating is very likely a result of the aging process. The Scanning Electron Microscope (SEM) image confirms that the second area is intensively micro-cracked. Potential influences of sample heating are discussed in section 4.2.

During our investigations with the SEM (see Appendix A.2.3), for some samples, the edge between the aged half and the unaged was found. For the 100 keV experiment we detected the edge as a change in contrast at the expected coordinates of the sample surface. For CFRP we also detected structural changes between the sample halves. Figure 8 shows the SEM image of CFRP. The plain gray area is the resin material, while the sharp black lines are the carbon fibres themselves. A diagonal pattern is visible which is a result of the production process. In the zoom image one can see the edge clearly in contrast and structural altering. The described phenomenon was not observed for the 2.5 keV experiment samples. Here, we could only find a contrast edge for CFRP under high magnification and no structural differences between the left and right sample side. Using the white light source of the Nomarski microscope (see Appendix A.2.4) and the UV light source for the fluorescence microscope mode, more details about the edge area were revealed. For the 100 keV experiment, we found the edge as a slight shadow under fluorescence for PTFE and CFRP. For the 2.5 keV experiment, all samples revealed an edge under Nomarski and fluorescence. The position of the edge was compared with the position of the sample in the sample holder to confirm the findings. These were in perfect correlation.

3.3 Optical Surface Degradation

As in the previous experiment, we used our LAMBDA set-up for in-situ observations (see Appendix A.1.1). All samples were illuminated with a 633 nm red laser
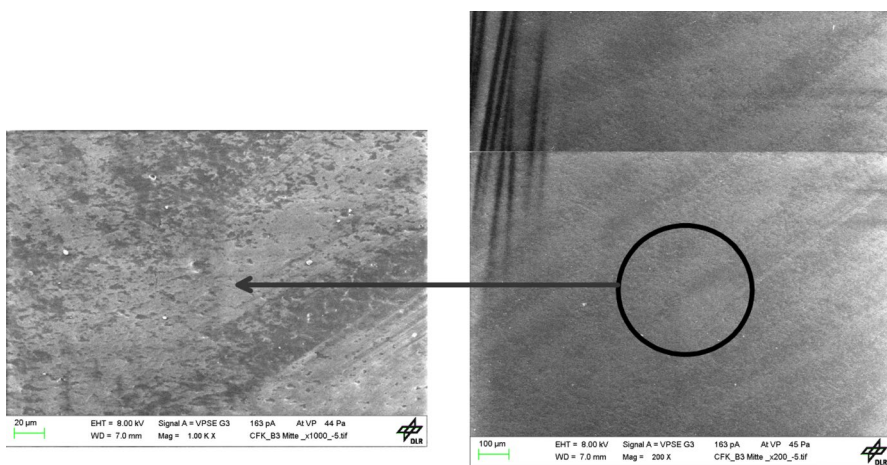

Fig. 8 SEM image of CFRP edge area (200× magnification) with zoom into the resin area (1000× magnification)

light source during proton irradiation. We took the average pixel value of each sample region in red channel of the RGB camera and plotted it over time. The blue and green channel were neglected since they are mainly recording noise and straylight of other sources, e.g. transom window. For the 100 keV experiment (Fig. 9), we detected changes, quantified by the slope of the linear data fit δ, for MLI and Acktar-Black, as well as slight changes for aluminum, titanium and the X-Ray film. The values for CFRP stayed steady during irradiation while a sudden increase in the beginning and the ending of the irradiation time is recognizable. This has already been observed in a previous experiment. This is suspected to be a surface charging effect. The raw image data of the 2.5 keV experiment shows randomly appearing sparkles, which is a further indication for this. During the whole measurement time, unirradiated regions labeled as "Reference" were observed and here, no peaks or changes in the pixel values were observed (Fig. 9, last row graphs "Reference 1" and "Reference 2"). The designated reference regions are image snippets of the plane copper sheet which is part of the sample holder assembly but not interacting with the proton beam.

Figure 10 was obtained during the 2.5 keV experiment. We find increasing sample brightness for CFRP and aluminum, constant sample brightness within the error range for Titanium and PTFE and decreasing sample brightness for AcktarBlack, coated Polyimide and X-Ray film. The AcktarBlack result is considered to be judged carefully since in its character as an ultra-black coating, its absorption coefficient is supposed to be higher than 99%. Due to the low signal, its data is supposed to underlie a high rate of uncertainty for all measurements.

The regions chosen as reference 1 and 2 both provide a $\delta \approx -0.3\%$ and $\delta \approx -0.5\%$ for both experiments respectively, which prove our method reliable and reproducible. Furthermore, we estimate this as measurement inaccuracy since this region
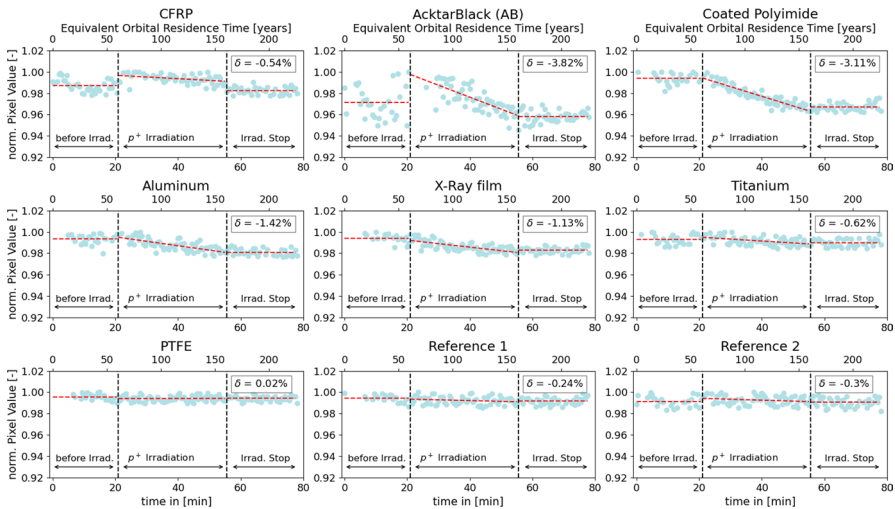

Fig. 9 Post-processed LAMBDA data collected during the 100 keV experiment (light blue dots: experiment data, red: linear fit)
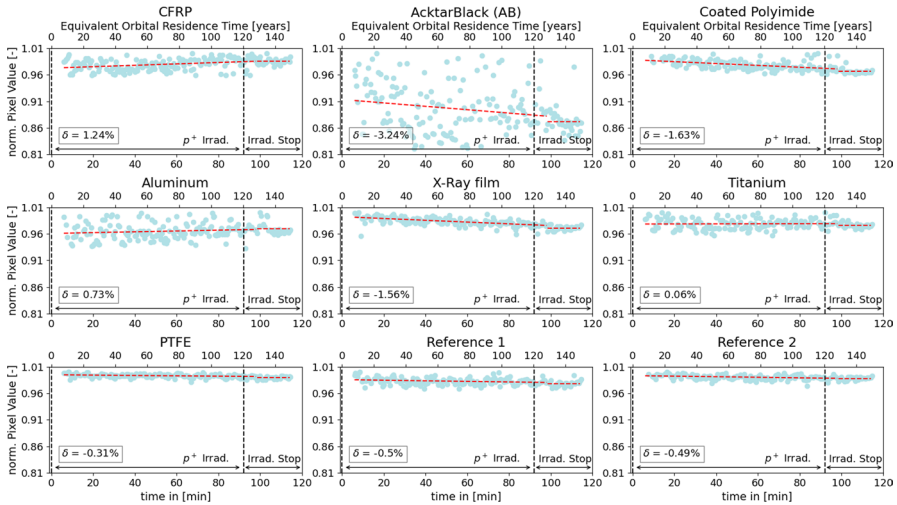
Fig. 10 Post-processed LAMBDA data collected during the 2.5 keV experiment (light blue dots: experiment data, red: linear fit)

should not change at all as it is not proton irradiated. Thus, we assume all data between 0% and −0.5% to be within the error range and therefore not to be a reliable result.

Directly after removing the samples from the chamber, we took retroreflectometer measurements (see Appendix A.2.2). They show minor changes in Solar Total Reflectivity for various samples in both experiments. Although, the results are within the given uncertainty range of the instrument, the trends line up well with the data, measured with LAMBDA. For the 100 keV experiment, the results range between 0 to 1.5% changes in reflectivity of the irradiated sample half, where the 1.5% is found for CFRP. The differences between covered and exposed sample half are approximately 3% for coated polyimide and 6% for CFRP, respectively. Furthermore, a change in Total Solar Reflectivity is detected for Aluminum with approximately 1%.

We also measured Fourier Transform Infrared (FTIR, see Appendix A.2.5) spectra of all samples over a wavelength range from 0.5 μm to 2.3 μm, which are shown in Fig. 11. As it already has been observed in the past [14], no significant variations in the samples' spectral features occur for both experiments. The spectra obtained of the 100 keV samples are plotted in Fig. 11. The values greater 1 in reflectivity for the IR region of coated polyimide is suspected to be due to a higher reflectivity than the copper standard as well as due to its uneven surface. The uneven surface appears as a result of taping the very thin foil to the sample holder.

Furthermore, we investigated the reflectivity change of each sample. Here, we put the unaged and aged sample half in relation and calculated a percentual value, displayed in Fig. 12. A positive change in reflectivity means that the aged sample half is more reflective, while a negative value stands for a reflectivity decrease. For the dark samples exposed to 100 keV protons, CFRP and AcktarBlack, (left panel, black
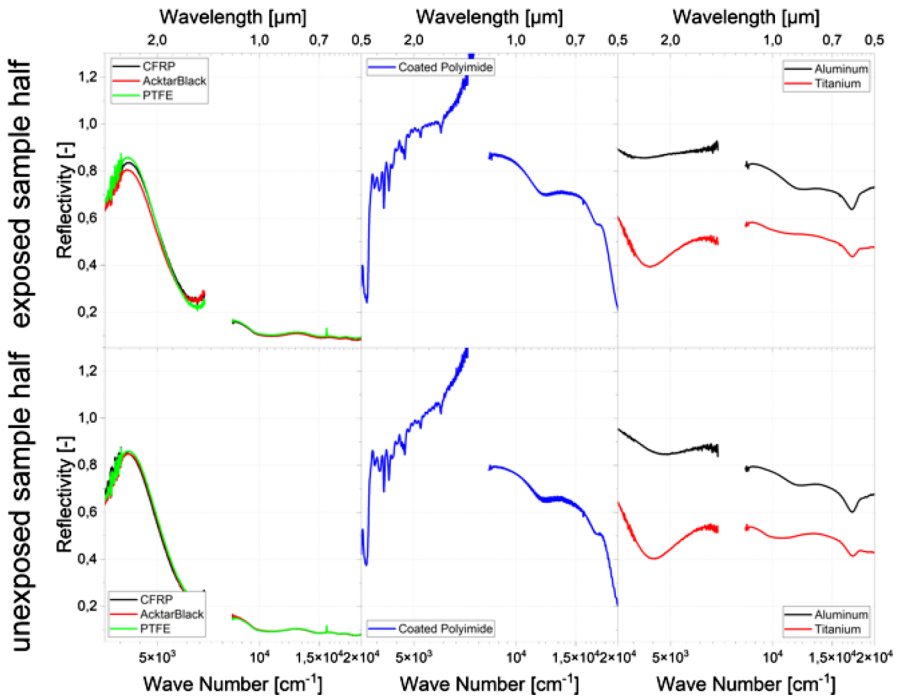
Fig. 11 Reflectivity spectra under 30° angle of incidence. Results for 100 keV p⁺ irradiation test

and red curve), minor reflectivity changes between ±7% in IR and between +5 and +10% in visible regions appear. Similar results have also been obtained for the 2.5 keV exposed samples. The changes on AcktarBlack are less than 2% while PTFE alternates between ±5% in both regions. CFRP range around 0 to -10% in the infrared, while it exceeds 10% in the visible region. The metallic samples, aluminum and titanium (Fig. 11 right panel, black and red curve), alternate between + 10 and − 10% after 100 keV exposure, while for 2.5 keV exposure the results are slightly more significant. Special attention is given to the coated Polyimide, where we observe recognizable reduction of the reflectivity after 2.5 keV exposure up to approximately ± 15% and recognizable less significant changes after 100 keV proton exposure. Here, we deal with a high uncertainty since the sample surface is not plain due to the adhesive tape that holds the foil in place. The edge areas have to be interpreted carefully as they underlie noise effects and therefore potential error propagation.

4 Discussion

4.1 Aging Effects by Visual Inspection

The irradiated areas of samples in experiment 1 (proton kinetic energy of 100 keV) showed no changes compared to the unirradiated areas in a visual inspection
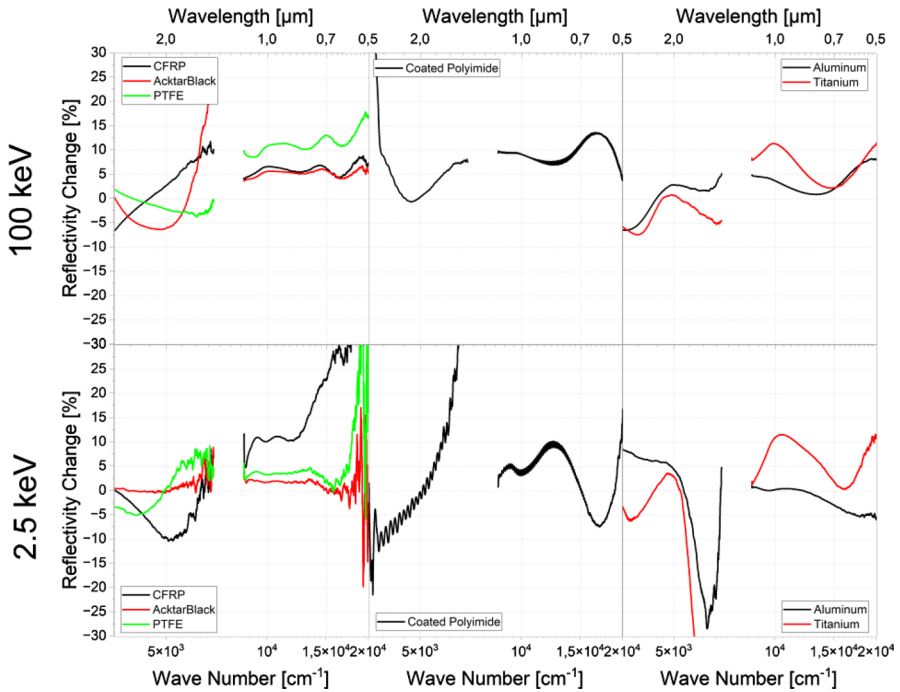
Fig. 12 Reflectivity changes (exposed/unexposed) induced by proton irradiation

performed immediately after removing samples from the complex irradiation facility. As opposed to this, the irradiated areas on samples from experiment 2 (proton kinetic energy of 2.5 keV) appeared slightly paler. This indicates a decrease in reflectivity and an increase in surface roughness. Also, chemical altering of the surface molecules is possible. We conclude more damage occurs closer to the sample surface for 2.5 keV than for 100 keV, since the penetration depth of the protons is a function of the proton energy. This is a reasonable result. Furthermore, we can conclude that the cover frame update was successful, since the optical investigation of the samples after irradiation showed a sharp edge between the exposed and unexposed halves. For further investigation we conclusively searched for this edge and took left and right sided data samples where necessary.

4.2 Mechanical Surface Degradation

As we found crack growth on the sample surface of AcktarBlack at 100 keV irradiation, we calculated the heating of the sample to exclude thermal tensions in the aluminum base material as a damage cause. Here, we made the conservative estimation that all energy of the proton beam is converted into sample heating. We assume thermal balance inside the sample and along the sample holder. Furthermore, we neglect heat dissipation due to radiation or conductivity. With these assumptions, we calculated

sample heating between 0.4 and 3 K in the 100 keV experiment and between 1.5 and 11 K for 2.5 keV for each sample individually. Due to the assumptions, this calculation provides an upper limit to the heating of the sample. As the temperature increase is not significant, surface damaging due to heat loads can be excluded. Therefore, we conclude that the detected damages are due to the proton interaction, which appear as micro-structural damages. We assume that the smaller penetration depth of the 2.5 keV lead do more damages near the surface and therefore cause the edge seen in the microscope. Since a certain acceleration of the SEM electrons are necessary, the penetration depth is exceeding the proton penetration depth for 2.5 keV, which leads to the conclusion that the damages are not measurable with that method. Our experiments simulate an in-orbit duration of 100 and 120 years, respectively, thus we conclude that mechanical surface degradation due to protons is minor and will be neglectable for ground-based observation of space debris.

4.3 Optical Surface Degradation

For the estimation of the optical surface degradation, we applied various methods. In direct comparison, the results of 100 keV and 2.5 keV were consistent within each method, whereas the results for 2.5 keV are more significant. We observe that irradiated materials become more diffusive after proton irradiation.

While the samples are still under irradiation, we observe surface charging effects, which could lead to the artifact of unsteady increase in brightness during LAMBDA measurements when the protons are released into the sample chamber. Heating effects are excluded due to the low, overall temperature increase.

The LAMBDA data are measured at 633 nm. Comparing this qualitatively with the FTIR data, the results agree well, as the reflectivity in the visible range is altered. The reflectometer measurements are in good agreement as well. Nevertheless, all reflectivity changes are in the narrow range of at maximum 15% for all materials in the FTIR under clean room conditions. A reasonable observation is that dark and diffuse samples tend to reflect better since their color changes to gray. The metals tend to be less reflective. For coated polyimide under 100 keV exposure we observe minor changes and an altering behaviour around 0 for the 2.5 keV exposure. The increasing reflectivity could be an indicator for a decaying ITO layer as it has reduced transmittivity in the visible region [17]. The reflectivity data for LAMBDA and the reflectometer are around 1%. Observed trends are in good agreement with all other collected data but still within the measurement tolerances of the devices. It needs to be noted that we assume no surface altering on the covered sample side due to appearing charging effects. Furthermore, the discussed results are in good conformity with our first experiment [14].

5 Conclusion

Six space related materials and a reference material were under investigation for their space aging behavior due to proton irradiation. We investigated the samples regarding their change in appearance, mechanical surface defects like crack growth

and their optical properties, in-situ and ex-situ. We found clearly visible changes of the sample appearance between the aged and unaged sample halves. Furthermore, we proofed mechanical damage on the AcktarBlack coating appearing as micro-cracking due to the proton interaction. Artifacts due to thermal effects were excluded. In-situ and ex-situ measurements show us a recognizable change in reflectivity of the sample surfaces. An interesting fact is that CFRP and aluminum samples appear brighter during proton irradiation, potentially due to charging effects, while all others decrease their brightness. Thus, an effect of surface charging on optical investigation of space objects can be neglected since the results range around a little under 2%. Considering atmospheric effects during observation of space debris from Earth, the relevance of brightness change due to surface charging is probably not given. We investigated the sample set with our FTIR spectrometer on a broad wavelength region. An overall damping of the sample reflectivity was measurable. The discrepancies between the aged and unaged sample halves are still insignificant and thus would not become relevant for telescopic investigation with ground-based telescopes. Therefore, we conclude that the interaction of surfaces with protons in the Inner Van-Allen-Belt are minor and will most certainly not affect spectrally resolved light curve data on a major scale.

Appendix A: Methods

A.1 In-Situ Measurements

A.1.1 Laser cAMera AlBeDo Analyzer LAMBDA

Our laser-based monitor system for in-situ tracking of surface altering was already introduced in detail in [14]. It consists of an expanded Helium-Neon-Laser (Melles Griot, 25-LHP series, 5 mW) at 633 nm and a camera. The installation is displayed in Figure 1. For the 100 keV experiment, the applied camera was a Canon Type EOS 5D Mark IV, while we used a Canon EOS 800D for the 2.5 keV experiment. The expanded laser beam illuminates the samples in the chamber under a fixed angle of 30° from left and below. The camera is in plane with the sample holder under an in-plane angle of 30° as well. An iterative loop images the sample holder every 30 s. In the post processing, the red channel of the RGB image is extracted and the pixel area relating to the respective samples are isolated. For each frame the mean value per sample area is found, which creates the list datapoints per time step and aged material.

A.2 Ex-Situ Measurements

A.2.1 Microscope Keyence Digital Microscope Type VHX-7000 Series

The microscopic inspection of the optical surfaces was performed with an incident light microscope, which is a Keyence Digital Microscope Type VHX-7000 Series.

Therefore, the blocks with the sample material were bordered by blocks with grey standards to get a reference for further picture processing at DLR Stuttgart. Furthermore, we intended to create reproducibility of the image scene before and after the radiation. The improved set-up allowed for recreating the exact sample position on the stage table as well as for saving the proper illumination settings per position each.

A.2.2 Surface Optics 410Solar/ET100 reflectometer / emissometer

For the measurement the Surface Optics 410Solar/ET100 reflectometer / emissometer was used. It allows to measure thermal emittance, and total hemispherical reflectivity. It is equipped with exchangeable integrating spheres. The emittance between 0 and 1 is measured in the wavelength range from 1500 nm to 21000 nm, and the reflectivity from 330 nm to 2500 nm with an uncertainty of $\pm$ 0.03 at ambient temperature according to the data sheet.

A.2.3 Scanning Electron Microscope Zeiss EVO MA 10 with Electron Dispersive X-Ray extension Bruker QUANTAX 200 *SEM/EDX*

The applied Scanning Electron Microscope (SEM) system is a Zeiss type EVO MA 10 with an Electron Dispersive X-Ray (EDX) extension from Bruker type QUANTAX 200. The SEM/EDX is applied to further investigate the sample surface structure as well as the surface material composition, aiming for identifying preferred elements to diffuse during proton irradiation. Furthermore, we were searching for sputtered copper and aluminum fragments to sort out potential artefacts resulting during irradiation.

A.2.4 Nomarski Microscope Olympus BX61

To further investigate on the surfaces, we applied a Nomarski microscope made by Olympus, type BX61, equipped with a UC90 color camera and a XM10 black and white camera. As light sources, a 100 W mercury-vapor light source and a 100 W halogen light source are available. The principle of the Nomarski microscope offers a more detailed inspection of surface altering since Nomarski Microscopes are working on an interference-based principle, which allows for an imaging of sample surface with very low contrasts.

A.2.5 Fourier Transform Infrared Spectrometer Bruker Vertex 70v

For obtaining spectral resolved reflectivity data on the sample surface we applied a Fourier Transform Infrared Spectrometer (FTIR) by Bruker Type Vertex 70v. The applied light sources are a Globar Infrared light source and a Wolfram white light source for the visible region. The related detector diodes are a DTGLaS diode for infrared (12000 - 250 cm^{-1}) and a silicon diode for the visible wavelength (25000 - 9000 cm^{-1}). To measure the reflectivity spectra, we used a mirror stage with 30° angle of incoming/outgoing light. The sample itself is placed on the table top, where

is a hole with 4 mm. The measurements where conducted in vacuum with a gold reference, as well as under air with a copper reference. The measurements under air are meant to provide data for comparison with the initial experiment in 2019, while the authors where hoping to improve the data quality by applying vacuum. The relativity of the measurement results was later on mathematically removed by multiplying the spectral data with a standard copper and gold spectrum.

Data availability Data availability upon reasonable request.

Declarations

Conflict of interest The authors declare that they have no conflict of interest.

References

1. Chow, D., Mitchell, A.: Astronauts take shelter as debris passes dangerously close to space station. NBC news. (2021) https://www.nbcnews.com/science/space/astronauts-take-shelter-debris-passes-dangerously-close-space-station-rcna5617
2. Dennison, J.R., Prebola, J., Evans, A., et al.: Comparison of flight and ground tests of environmental degradation of MISSE-6 SUSpECS materials. IEEE Trans. Plasma Sci. **40**(2), 254–261 (2012). https://doi.org/10.1109/TPS.2011.2178104
3. Dever, J.A., Miller, S.K., Sechkar, E.A., et al.: Space environment exposure of polymer films on the materials international space station experiment: results from MISSE 1 and MISSE 2. High Perform. Polym. **20**(4–5), 371–387 (2008). https://doi.org/10.1177/0954008308089704
4. Dianetti, A.D., Crassidis, J.L.: Resident space object characterization using polarized light curves. J. Guid. Control Dyn. **46**(2), 246–263 (2023). https://doi.org/10.2514/1.G006847
5. Engelhart, D., Cooper, R., Cowardin, H., et al.: Space weathering experiments on spacecraft materials. J. Astronaut. Sci. **66**(2), 210–223 (2019). https://doi.org/10.1007/s40295-019-00175-2
6. Engelhart, D.P., Reyes, J.A., Murray, V.G., et al.: Identifying radiation induced spectroscopic changes in polyimide materials. J. Astronaut. Sci. **69**, 164–174 (2022). https://doi.org/10.1007/s40295-021-00291-y
7. ESA Space Debris Office: ESA's annual space environment report. Tech. rep. GEN-DBLOG-00288-OPS-SD (2022). https://www.sdo.esoc.esa.int/environment_report/Space_Environment_Report_latest.pdf
8. Ganushkina, N.Y., Dandouras, I., Shprits, Y., et al.: Locations of boundaries of outer and inner radiation belts as observed by cluster and double star. J. Geophys. Res. **116**, A09234 (2011). https://doi.org/10.1029/2010JA016376

9. Heynderickx, D., Quaghebeur, B., Evans, H.: The ESA space environment informationsystem (SPENVIS). In: IAF abstracts, 34th COSPAR Scientific Assembly. id. 475 (2002). https://doi.org/10.2514/6.2000-371

10. Hyde, J., Christiansen, E. and Lear, D.: Observations of micrometeoroid and orbital debris impact damage to the International Space Station. In: First International Orbital Debris Conference, ID #6001 (2019). https://www.hou.usra.edu/meetings/orbitaldebris2019/orbital2019paper/pdf/6001.pdf

11. IADC. Sensor systems to detect impacts on spacecraft, Inter-Agency Space Debris Coordination Committee, Work Group 3, No. IADC-08-03 (2013)

12. Jordan, C.E.: NASA radiation belt models AP-8 and AE-8. Tech. rep., Radex Inc. Bedford, MA (1989). https://apps.dtic.mil/sti/citations/tr/ADA223660

13. Kabayashi, D., Frueh, C.: Reformulating compressed sensing to be used with semiresolved point spread function and light curves for space object imaging: LEO. In: AMOS Advanced Maui Optical and Space Surveillance Technologies Conference (2022). https://amostech.com/TechnicalPapers/2022/Poster/Kobayashi.pdf

14. Keil, D., Seiz, F., Bartels, N., et al.: Surface modification of space exposed materials induced by low energetic proton irradiation. J. Astronaut. Sci. 68(4), 1170–1185 (2021). https://doi.org/10.1007/s40295-021-00277-w

15. Ley, W., Wittmann, K., Hallmann, W.: Handbuch der Raumfahrttechnik, 4th edn. Carl Hanser Verlag, München (2011)

16. Malik, T.: Russia to launch new Soyuz capsule to replace leaky spacecraft on space station. Spacecom (2023). https://www.space.com/russia-replacement-soyuz-launching-february-2023

17. Meraz Davila, S., Chávez Urbiola, I., Párez, C., et al.: Solution processable P3HT/CdS photodiodes and their electrical characterization. Int. J. Electrochem. Sci. 11, 2962–2970 (2016). https://doi.org/10.20964/110402962

18. NIST National Institute for Standards and Technology (2023) PSTAR. Web Tool, https://physics.nist.gov/PhysRefData/Star/Text/PSTAR.html

19. Nöldeke, C.: The space radiation environment. epubli (2017)

20. Nussbaum, M., Schafer, E., Yoon, Z., et al.: Spectral light curve simulation for parameter estimation from space debris. Aerospace 9(8), 403 (2022). https://doi.org/10.3390/aerospace9080403

21. Plis, E.A., Engelhart, D.P., Cooper, R., et al.: Review of radiation-induced effects in polyimide. Appl. Sci. 9(10), 1999 (2019). https://doi.org/10.3390/app9101999

22. Renger, T., Sznajder, M., Witzke, A., et al.: The complex irradiation facility at DLR-Bremen. In: Macdonald, M. (ed.) Advances in Solar Sailing. Springer, Berlin, Heidelberg (2014). https://doi.org/10.1007/978-3-642-34907-2_34

23. Richter, H., Buchbender, C., Güsten, R., et al.: Direct measurements of atomic oxygen in the mesosphere and lower thermosphere using terahertz heterodyne spectroscopy. Commun. Earth Environ. 2(1), 19 (2021). https://doi.org/10.1038/s43247-020-00084-5

24. Scharring, S., Kästel, J.: Can the orbital debris disease be cured using lasers?. Aerospace 10(7), 633 (2023). https://doi.org/10.3390/aerospace10070633

25. Scharring, S., Kästel, J., Wagner, G., et al.: Potential of using ground-based high-power lasers to decelerate the evolution of space debris in LEO. In: 8th European Conference on Space Debris (2021). https://conference.sdo.esoc.esa.int/proceedings/sdc8/paper/98/

26. Scharring, S., Eisert, L., Lorbeer, R.A., et al.: Momentum predictability and heat accumulation in laser-based space debris removal. Opt. Eng. 58(1), 011004 (2018). https://doi.org/10.1117/1.OE.58.1.011004

27. Sicard, A., Boscher, D., Bourdarie, S., et al.: GREEN: the new Global Radiation Earth ENvironment model (beta version). Ann. Geophys. 36, 953–967 (2018). https://doi.org/10.5194/angeo-36-953-2018

28. Skurat, V., Barbashev, E., Dorofeev, Y.I., et al.: Simulation of polymer film and surface behaviour in a space environment. Appl. Surf. Sci. 92, 441–446 (1996). https://doi.org/10.1016/0169-4332(95)00273-1

29. Strickland, A.: Space junk hit the International Space Station, damaging a robotic arm. CNN Cable News Network https://edition.cnn.com/2021/06/01/world/iss-orbital-debris-robotic-arm-scn/index.html (2021)

30. Stryjewski, J., Hand, D., Tyler, D., et al.: Real time polarization light curves for space debris and satellites. In: Advanced Maui Optical and Space Surveillance Technologies Conference, E39 (2010)

31. Sunseri, G., Martinez, L.: Satellite collision puts Hubble at risk. abc NEWS (2009). https://abcne ws.go.com/Technology/Space/story?id=6867190 &page=1
32. Tingley, B. International Space Station fires thrusters to dodge space junk. Spacecom (2023). https://www.space.com/international-space-station-dodge-space-junk-march-2023
33. Wall, M.: Hole in leaky Russian Soyuz spacecraft not caused by Geminid meteor. Spacecom (2022). https://www.space.com/russian-soyuz-spacecraft-leak-not-geminid-meteor
34. Yi, G.T., de Groh, K.K., Banks, B.A., et al.: Overview of the MISSE 7 polymers andzenith polymers experiments after 1.5 years of space exposure. In: International Symposium on Materials in the Space Environment (ISMSE-12), NASA/TM-2013-217848 (2013). https://ntrs.nasa.gov/citat ions/20130011784
35. Ziegler, J.F., Ziegler, M.D., Biersack, J.P.: SRIM - The stopping and range of ions in matter (2010). Nucl. Instrum. Methods Phys. Res. B **268**(11–12), 1818–1823 (2010). https://doi.org/10. 1016/j.nimb.2010.02.091